

# Inverse Mapping for Rainfall-Runoff Models using History Matching Approach

Natalia V. Bhattacharjee<sup>a,b</sup>, Pritam Ranjan<sup>c</sup>, Abhyuday Mandal<sup>b,\*</sup>, Ernest W. Tollner<sup>a</sup>

<sup>a</sup>College of Engineering, University of Georgia, Athens, USA

<sup>b</sup>Department of Statistics, University of Georgia, Athens, USA

<sup>c</sup>OM&QT, Indian Institute of Management Indore, MP, India

---

## Abstract

In this paper, we consider two rainfall-runoff computer models. The first model is Matlab-Simulink model which simulates runoff from windrow compost pad (located at the Bioconversion Center in Athens, GA) over a period of time based on rainfall events. The second model is Soil Water Assessment Tool (SWAT) which estimates surface runoff in the Middle Oconee River in Athens, GA. The input parameter spaces of both models are sensitive and high dimensional, the model output for every input combination is a time-series of runoff, and these two computer models generate a wide spectrum of outputs including some that are far from reality. In order to improve the prediction accuracy, in this paper we propose to apply a history matching approach for calibrating these hydrological models, which also gives better insights for improved management of these systems.

*Keywords:* Calibration, Contour estimation, Gaussian process model, Prediction, SWAT

---

## 1. Introduction

Composting is one of the effective methods of organic material decomposition [Kalaba et al., 2007]. The composting pad runoff must be collected into a pond prior to its further use since the composting systems are usually located in remote areas [Dorahy et al., 2009]. Traditionally applied curve number method for predicting runoff from rainfall events is very site specific and not realistic for forecasting runoff from windrow composting pad [Tollner and Das, 2004]. Consequently, a good hydrologic design and compost pad management are required as pond sizing and the runoff water quality are highly regulated [Bhattacharjee and Tollner, 2016]. For the state of Georgia, USA, composting is an important option of interest as there are forty to fifty windrow composting systems in Georgia. Management of the composting pad is crucial since the pad runoff is highly

---

\*Corresponding author

*Email address:* amandal@stat.uga.edu (Abhyuday Mandal)

regulated and researchers tried to estimate runoff in order to provide guidance for retention pond design [Kalaba et al., 2007, Wilson et al., 2004]. The first computer model of interest is a Matlab-Simulink compartmental dynamic model that estimates the amount of runoff from the windrow composting pad [Duncan et al., 2013a].

The second model, Soil and Water Assessment Tool (SWAT) is a complex hydrological model that simulates runoff from watershed areas based on climate variables, soil types, elevation and land use data [Arnold et al., 1994]. It is an internationally accepted simulator and used in modeling of the rainfall-runoff processes across various watersheds and river basins to address climate changes, water quality, land use and water resources management practices [Krysanova and Srinivasan, 2015, Dile et al., 2013, Jayakrishnan et al., 2005, Srinivasan et al., 2005]. Sequential Uncertainty Fitting (SUFI2) is one of the methods used in SWAT-CUP (Soil and Water Assessment Tool Calibration and Uncertainty Procedures) for calibration and uncertainty analysis [Abbaspour et al., 2004, 2007]. Calibrating these models are challenging since these simulators give a wide spectrum of output series and calibration procedures require significant amount of time. The objectives here are to effectively find the best combination of the input parameters that improves runoff modeling and contribute to better management practices.

From a statistical standpoint, this model parameter estimation problem simplifies to finding an inverse solution of a computer simulator that generates pre-specified time-series output (i.e., realistic output series). For the application at hand, the computer simulators are the Matlab-Simulink compartmental model and the SWAT model. Here, a simulator takes a  $d$ -dimensional vector as input and returns a time-series output. Mathematically, suppose the simulator output is denoted by  $g(x) := \{g(x, t), t = 1, 2, \dots, T\}$  for a given input  $x \in [0, 1]^d$  (scaled to an unit cube for convenience), then the objective is to find the  $x$  (or set of  $x$ 's) that generate the desired (pre-specified) output  $g_0 := \{g_0(t), t = 1, 2, \dots, T\}$  (say). Figure 1 represents illustration of the main idea behind computer experiments – the experimentation with computer simulators. Assuming that a realistic computer simulator of a complex physical process is also computationally and/or financially expensive, a statistical surrogate is often used to emulate the simulator outputs and provide inference about physical experiments. In this paper, we propose to use history matching algorithm [Vernon et al., 2010] for solving this inverse mapping problem for the rainfall-runoff models.

For time-series response of a simulator, Vernon et al. [2010] proposed an iterative approach called history matching (HM) for calibrating a cosmological simulator GALFORM – a galaxy

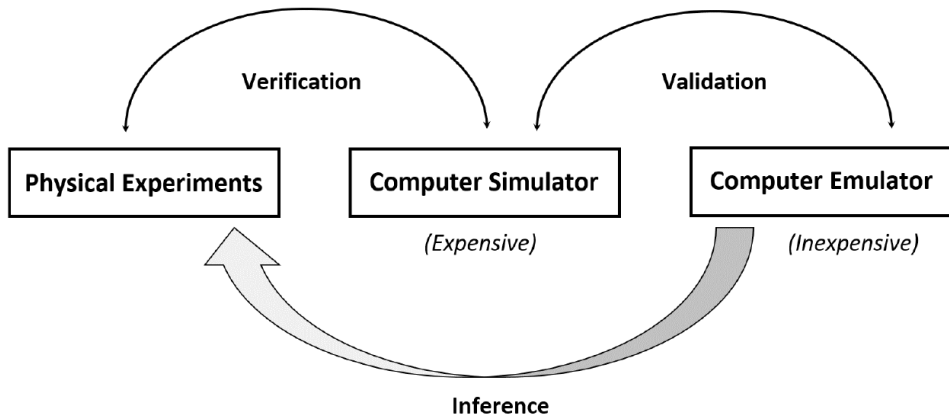


Figure 1: Illustration of computer experiments

formation model. HM algorithm cleverly eliminates the implausible points from the input (or parameter) space and returns a set of plausible candidates for the inverse solution. However there are a few aspects of the HM algorithm by Vernon et al. [2010] that differs from our objective. Note that the end result of the HM algorithm may be an empty set if there does not exist an inverse solution. Moreover, the HM algorithm requires a large number of simulator runs which is undesirable in several applications like ours, where the simulator is expensive to evaluate. Thus, we propose a modification in the HM algorithm which requires fewer simulator runs.

The remainder of the manuscript is organized as follows: Section 2 sets up the two motivating examples of our study (Matlab-Simulink and SWAT models) for which we want to solve the inverse problems. Section 3 presents the methodology for the proposed history matching algorithm for solving the inverse problems. The implementation of the proposed strategy is shown for the two motivating examples in Section 4, and Section 5 concludes the article with a summary and important remarks. We also present supplementary material with more methodological details and simulation study results for interested readers.

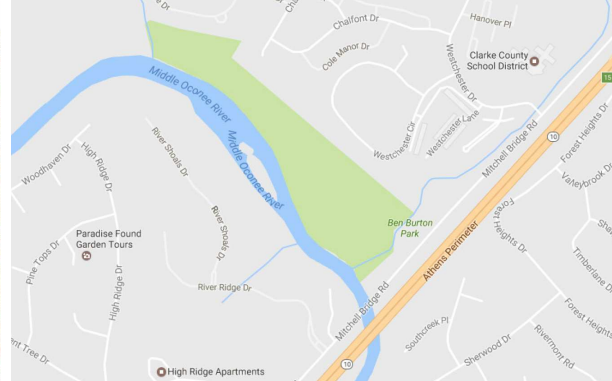
## 2. Motivating Application

In this paper, we discuss the calibration of two rainfall-runoff computer simulators for two target data sets collected at different locations in Athens, (1) the Bioconversion center, UGA, and (2) the Middle Oconee River, respectively (Figure 2 shows the two sites).

For the Bioconversion center, UGA, we use the runoff data ( $g_0$ ) collected on a 10-minute interval during 11:50AM, December 23, 2010 to 11:50PM, January 30, 2011, that is,  $T = 5445$  time points



(a) Bioconversion center, UGA, Athens



(b) Middle Oconee River near Ben Burton Park

Figure 2: Rainfall-runoff dynamics study site locations in Athens, Georgia, USA.

(the noisy red curve in Figure 4). The measurements were taken using rain gauge data logger which was placed between the compost pad and collection pond. The pond stage measurements were recorded using two pressure transducers. Full description of data collection and characteristics of composting pad can be found in Duncan et al. [2013a,b].

For the Middle Oconee River data, the streamflow data during 2001 and 2009 were used for calibration with a warm-up period of 2 years (from January 2001 to December 2002). The data were retrieved from the U.S. Geological Survey (USGS) website (gauge number 02217500 located near Ben Burton Park, Athens, GA). There were total 84 observations (January 2003 – December 2009) (the red curve in Figure 6). Due to economic development in this area, there have been an increase in population and municipal water demand [Commission, 2011]. Additionally, Bastola and Misra [2015] observed large amount of rainfall, land use changes, climate variability and extremes in the southeast region of USA.

### 2.1. Matlab Simulink Model

Duncan et al. [2013a] investigated the rainfall-runoff relationship for the windrow composting pad, and proposed a compartmental dynamic model (Matlab-Simulink model) for estimating the amount of runoff from the composting pad. Figure 3 demonstrates the schematic representation of the compartmental model derived from a similar tank model that was developed to calculate the rate of runoff and sediment yield in a watershed [Lee and Singh, 2005].

In Figure 3, compartments 1 and 2 represent the up slope and down slope pad sections, respectively. The rainfall either infiltrates to the compartment 3 (gravel sub-surface) or becomes overland flow. The compartment 3 allows either deep infiltration or lateral flow.

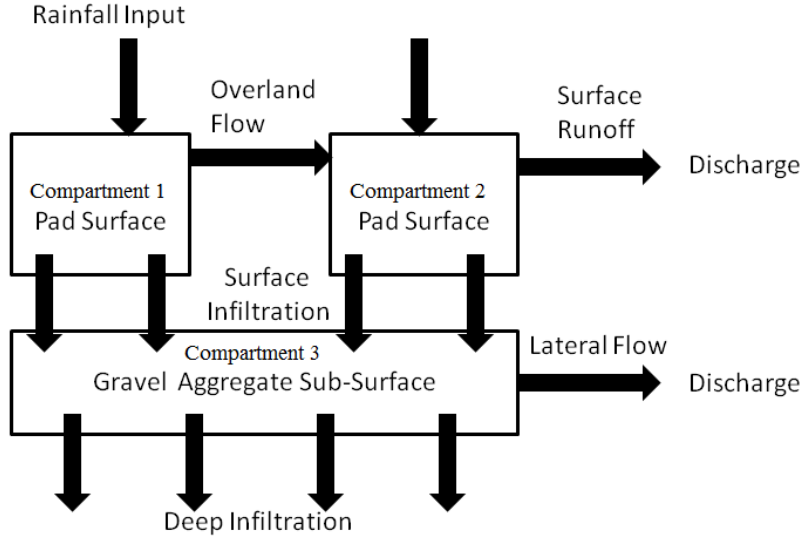


Figure 3: Schematic of cross-sectional view of composting pad at the Bioconversion center, UGA, Athens, USA.

This Simulink model takes several factors as inputs, for instance, length, width, slope of compost pad, area of compost piles, depth of surface/sub-surface, depression/embankment depths, initial surface/sub-surface water content, and a few model coefficients like  $K_{eff}$ ,  $K_{sat1}$  and  $K_{sat2}$ . Based on the expert’s opinion, four inputs ( $K_{sat1}$ ,  $K_{sat2}$ , depth of surface and depth of sub-surface) are considered as the most influential. For convenience in methodological implementations, the inputs were scaled to  $[0, 1]^4$ . The output variable of interest is the runoff, represented as a change in Pond Volume (recorded by the pressure transducer for pond stage measurements). Figure 4 shows a few random simulator outputs superimposed with the actual field data.

The objective here is to find the best possible combinations of the four parameters – two saturation coefficients ( $K_{sat1}$  and  $K_{sat2}$ ), surface depth and subsurface depth – that can generate realistic runoff, i.e., similar to the one obtained from the Bioconversion center at UGA. In other words, we need to find suitable inputs for the Matlab-Simulink model such that the blue curve obtained approximates the red one as close as possible (w.r.t. Figure 4).

## 2.2. SWAT model

SWAT model has been widely used for runoff modeling in a watershed in order to look at the effect of climate change, land use and water resources management practices [Arnold et al., 1994, Jayakrishnan et al., 2005, Srinivasan et al., 2005, Dile et al., 2013, Krysanova and Srinivasan, 2015] on streamflow and water quality. Figure 5 shows the schematics of the SWAT model we use in

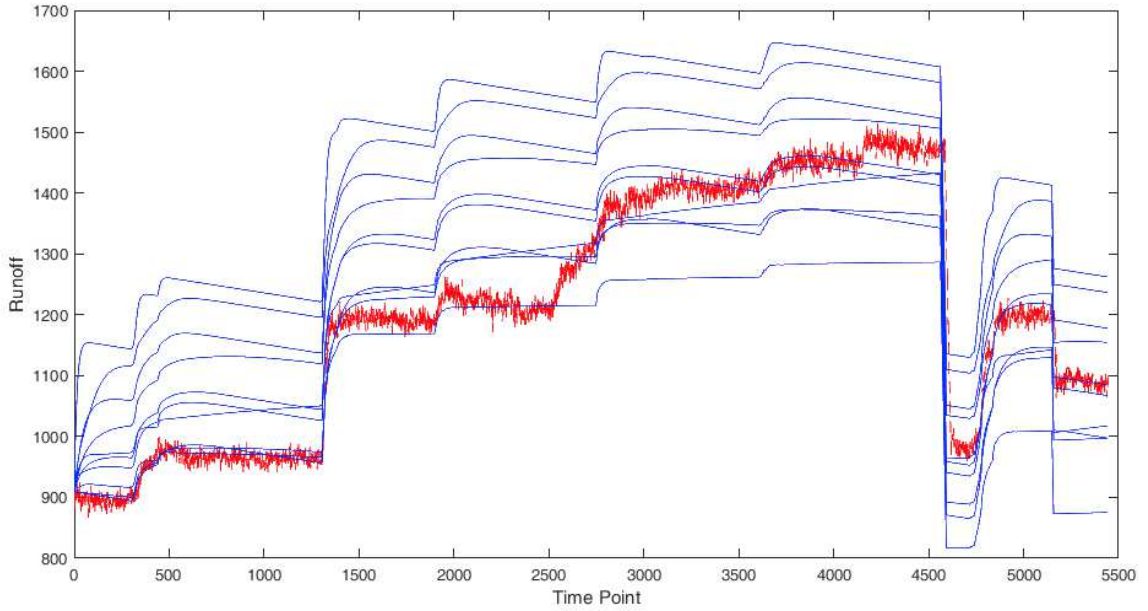


Figure 4: Actual runoff data ( $g_0(t)$ ) from Bioconversion center, UGA, (during Dec 2010 – Jan 2011), and the Matlab-Simulink model outputs  $g(x, t)$  for  $t = 1, 2, \dots, 5445$  at ten randomly generated  $x$  in  $[0, 1]^4$ .

this paper. This hydrological model takes inputs from climate data (rainfall, air temperature,

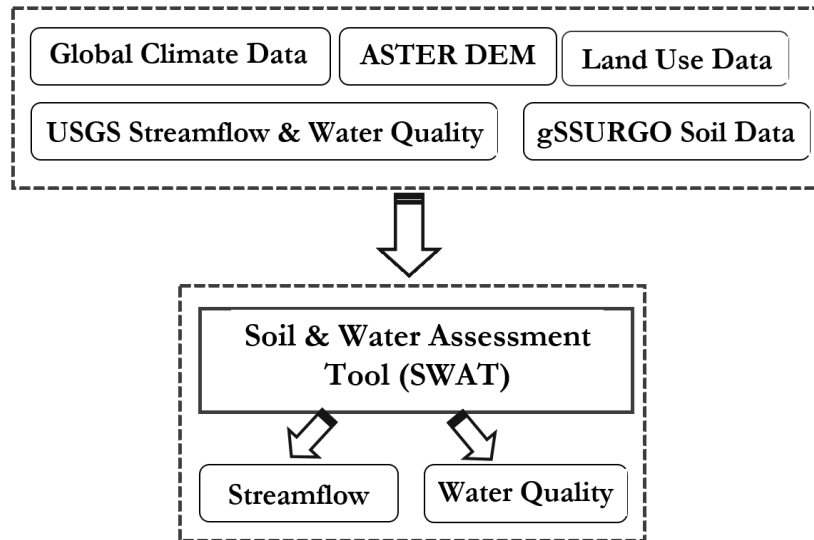


Figure 5: Conceptual representation of SWAT model.

solar radiation, relative humidity and wind speed), digital elevation model (DEM) data, land use

and soil type data. Historical monthly data of streamflow were retrieved from the US Geological Survey (USGS) water data website for gauge number 02217500. We used USGS EarthExplorer data download platform to obtain ASTER DEM at 30 m resolution for our study area. We used National Land Cover Database (NLCD) website to download land cover data for 2001 year. For the soil type data, we used Soil Survey Geographic Database (gSSURGO). Additionally, we used Global Climate Data in SWAT format from Texas A&M University website (<https://globalweather.tamu.edu/>).

In this paper, we first identify the important parameters of SWAT model using Sequential Uncertainty Fitting (SUF12) toolkit. We considered  $p$ -value  $< 0.05$ , coefficient of determination  $R^2 > 0.5$  and Nash-Sutcliffe efficiency ( $NSE$ ) coefficient  $> 0.5$  as the acceptable values. In this analysis, out of initial twenty six parameters, five parameters turned out to be important: Manning’s  $n$  for the main channel  $\in (0, 0.3)$ , effective hydraulic conductivity in the main channel  $\in (0, 130)$ , groundwater delay  $\in (0, 500)$ , groundwater “revap” coefficient  $\in (0, 0.2)$  and available water capacity  $\in (-0.2, 0.4)$ . We then solve inverse problem for this reduced model w.r.t. these five parameters using both SUF12 [Abbaspour et al., 2004, 2007] and history matching based approach. Figure 6 illustrates a few SWAT model runs obtained by varying these five parameters and the actual field monthly data recorded at the Middle Oconee River (USGS gauge number 02217500) during the period from January 2003 to December 2009.

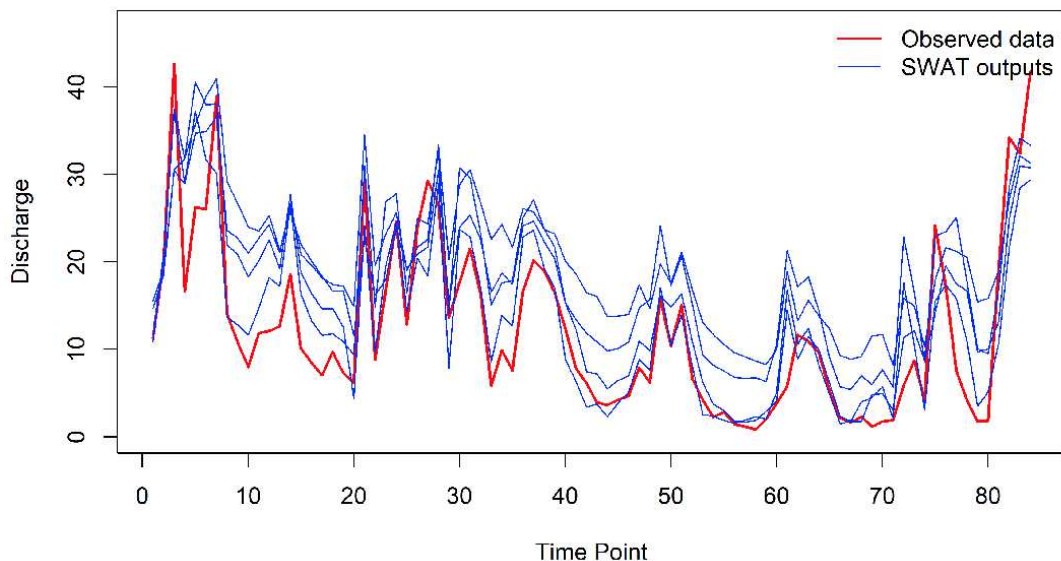


Figure 6: Actual streamflow data,  $g_0(t)$ , USGS gauge from the Middle Oconee River near Burton Park, Athens, (during 2003 – 2009), and SWAT model outputs  $g(x, t)$  for  $t = 1, 2, \dots, 84$ , at five randomly generated  $x$  in  $[0, 1]^5$ .

Thus, the objective here is to find the set of these five inputs that can generate simulator

outputs as close as possible to the target – actual data from the Middle Oconee River. Recently, the calibration and uncertainty analyses of SWAT model has been investigated by [Abbaspour et al., 2004, 2007] in SWAT-CUP. In this paper, we investigate the calibration of SWAT model using the proposed history matching algorithm.

### 3. Methodology

In this paper, we primarily focus on the history matching (HM) approach proposed by Vernon et al. [2010]. As mentioned in Section 1, we apply the HM algorithm with a variation which allows us to find the inverse solution in fewer simulator runs, and give us a perfect match if possible, or the best approximation instead of returning an empty set of inverse solutions. For a benchmark comparison of the proposed HM approach, we use a rather simple scalarization method proposed by Ranjan et al. [2016]. See Supplementary Material section for details on the scalarization method, and the most important tool in building statistical surrogates – Gaussian process (GP) models. These GP models are also extensively used in the HM algorithm.

In a nutshell, the history matching algorithm proposed by Vernon et al. [2010] discretizes the time-series response on  $T_k$  time points, say, at  $t_1^*, t_2^*, \dots, t_{T_k}^*$ , such that  $T_k \ll T$ , but these  $T_k$  time points capture the defining features of the target response, and then find a common set of plausible solutions to  $T_k$  inverse problems for scalar-valued simulators. In other words, it boils down to finding  $x \in [0, 1]^d$  such that  $g(x, t_j^*) = g_0(t_j^*)$  for all  $j = 1, 2, \dots, T_k$ . The driving force behind this approach is the implausibility function

$$I_{(j)}(x) = \frac{|\hat{g}(x, t_j^*) - g_0(t_j^*)|}{s_{t_j}(x)},$$

where  $\hat{g}(x, t_j^*)$  and  $s_{t_j}(x)$  are the predicted mean response and the associated uncertainty estimate, respectively, obtained from a GP model fitted to the scalar valued simulator  $g(x, t_j^*), x \in [0, 1]^d$  on a training set. Vernon et al. [2010] further proposed an iterative approach to refine the plausible subset of points from the input space. However, the algorithm is designed to find the set of all plausible inverse solutions and not only the perfect solution. For their Galaxy formation model application with input dimension  $d = 17$ , Vernon et al. [2010] used a large training set to start with ( $n_1 = 1000$ ) and ended up with  $N = 2011$  points after four iterations.

We propose a few modifications in their history matching algorithm so that we find only the best possible approximation of the inverse solution instead of the entire plausible set, and prefer to use a reasonably small space-filling design instead of a large design in  $[0, 1]^d$  for building the



initial surrogate. For instance, the rule of thumb by Loepky et al. [2006] suggests that 10 points per input dimension should be enough for getting an overall idea of the underlying process (i.e.,  $n_1 = 10d$ , where  $d$  is the input dimension). The key steps of the proposed HM algorithm are summarized as follows:

1. Choose a discretization-point-set (DPS),  $t_1^*, t_2^*, \dots, t_{T_k}^*$ .
2. Set  $i = 1$ . Assume  $D_0 = \phi$  (empty set).
3. Choose a training set,  $D_1 = \{x_1, x_2, \dots, x_{n_1}\} \subset [0, 1]^d$ , using some space-filling design scheme like maximin Latin hypercube, and evaluate the original simulator  $g(x)$  over  $D_1$ .
4. Fit  $T_k$  scalar-response GP models to  $g(x, t_j^*)$  over the training set  $D = D_i \cup D_{i-1}$ .
5. Evaluate the implausibility criteria  $I_{(j)}(x)$  for  $j = 1, 2, \dots, T_k$  over a randomly generated test set  $\chi_i$  of size  $M$  (via a space-filling design) in  $[0, 1]^d$  and combine them via

$$I_{max}(x) = \max\{I_{(1)}(x), I_{(2)}(x), \dots, I_{(T_k)}(x)\},$$

for screening the plausible set of points  $D_{i+1} = \{x \in \chi_i : I_{max}(x) \leq c\}$ . The cutoff  $c$  is generally pre-decided, for instance, based on  $3\sigma$  rule of thumb.

6. Stop if  $D_{i+1} = \phi$ , otherwise, set  $i = i + 1$ , evaluate the simulator on  $D_i$  and go to Step 4.

Since we assume that the target response is a realization of the simulator output, one can find the inverse solutions via the Euclidean distance approach, i.e., the point  $x \in [0, 1]^d$  with the smallest

$$d(x) = \sqrt{\sum_{j=1}^{T_k} |\hat{g}(x, t_j^*) - g_0(t_j^*)|^2}$$

based on the final fit can be a decent approximation. Alternatively, one can use the minimizer of  $d_2(x_i) = \|g(x_i) - g_0\|$  over  $x_i \in D$  as a good approximation of the desired inverse solution.

Note that the efficiency of the HM algorithm depends on the appropriate choice of DPS, and the test-set size  $M$ . Based on our empirical findings via a simulation study, we infer that the size of the test-set gives a trade-off between large training-set ( $N$ ) and accuracy of the inverse solution. The size and value of DPS should be determined from the expert's prior belief and perhaps a pilot study of the computer simulator. Due to the stochastic nature of the HM algorithm, a multi-start approach of the proposed HM algorithm may lead to improved accuracy, however one must analyze the tradeoff between the accuracy gain and the additional cost of simulator evaluation for the application at hand. In our paper, we repeated the process 10 times.

Please refer to the Supplementary Materials section for a step-by-step illustration of the proposed HM approach on a toy example, along with some simulation studies to investigate the sensitivity of our approach.

#### 4. Implementing the Applications

##### 4.1. Matlab-Simulink Application

Recall that the objective here is to find the input settings (combinations of  $K_{sat1}$ ,  $K_{sat2}$ , depth of surface and depth of sub-surface) for the simulator that generate the target runoff. We applied the proposed HM algorithm for solving the underlying inverse problem with  $T_k = 4$ ,  $n_1 = 40$ ,  $c = 3$ ,  $M = 5000$ , and  $DPS = (135, 554, 1243, 3232, 4500)$ . These settings were chosen based on the findings of a simulation study of an illustrative example (see Supplementary Material section) and some advice from the application expert. The performance of a method is evaluated by Root Mean Square Error,

$$RMSE = \sqrt{\frac{\sum_{t=1}^n [g_0(t) - g(x_0, t)]^2}{n}}.$$

The lower the RMSE value, the better the model is. As evident from Figure 7, which shows the best solutions for the two approaches and the target solution, the result of the HM approach is significantly better than that of the compartment model. The compartment model fit has the RMSE of 71.91 whereas that of the HM approach is only 55.58 (with  $N = 461$  function evaluations), indicating a  $(71.91 - 55.58)/55.58 \times 100 \approx 30\%$  improvement. We also computed other goodness-of-fit statistics such as Nash-Sutcliffe Efficiency and the  $R^2$  between the observed data and the predicted values for both of the compartment model and HM approach. These numbers, given in Table 1, also indicate the better performance of the proposed HM method.

##### 4.2. SWAT model

We apply the proposed HM algorithm to find the best combinations of Manning's  $n$ , effective hydraulic conductivity (EHC), groundwater delay (GWD), groundwater delay time (GDT) and available water capacity (AWC), and compare the results obtained from SUFI2 [Abbaspour et al., 2004, Arnold et al., 2012]. The key factors of the proposed HM algorithm were  $T_k = 4$ ,  $n_1 = 50$ ,  $c = 3$ ,  $M = 5000$ , and  $DPS = (10, 43, 57, 79)$ . The proposed HM algorithm required  $N = 387$  model runs in order to find the best solution. We plot the target solution along with the best

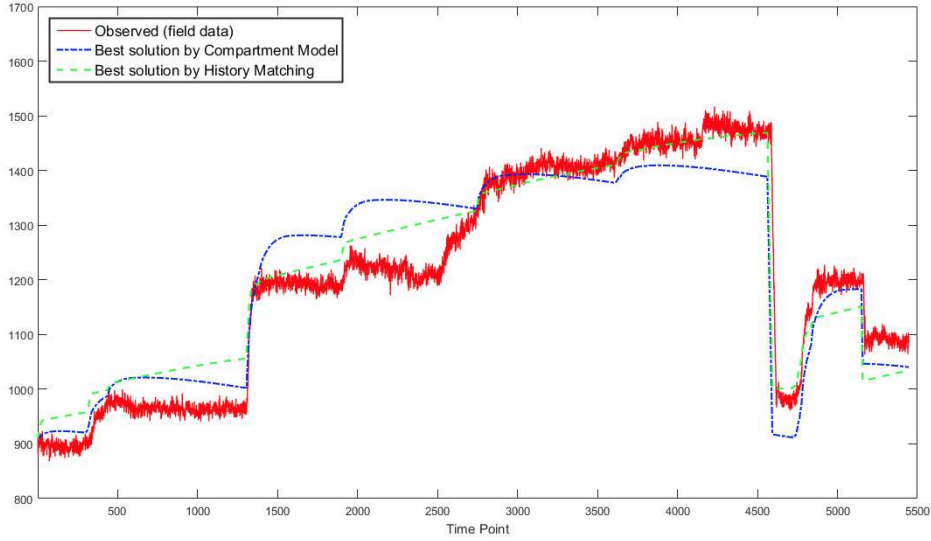


Figure 7: Calibration Results for the Matlab-Simulink model. The solid red curve represents observed data, blue dash line represents best solution using compartment model and green dash line corresponds to the best solution using the proposed history matching algorithm.

solutions obtained by SUFI2 and HM algorithms (Figure 8). Again the HM algorithm performed better and resulted in  $RMSE$  value of 4.70. Here the  $RMSE$  of SUFI2 is 5.21 which indicates a  $(5.21 - 4.70)/4.70 \times 100 \approx 11\%$  improvement. The  $NSE$  and  $R^2$  values of SUFI2 and HM, given in Table 1, also suggest that the HM approach performs better.

## 5. Summary and Conclusion

In this study, we applied a modified history matching (HM) algorithm for calibrating two computer models (Matlab-Simulink and SWAT). With implementation of both models, HM algo-

Table 1:  $NSE$ ,  $R^2$  and  $RMSE$  comparisons for different models

		$NSE$	$R^2$	$RMSE$
Simulink	Compartment	0.86	0.86	71.71
	HM	0.92	0.93	55.58
SWAT	SUFI2	0.72	0.74	5.21
	HM	0.77	0.78	4.70

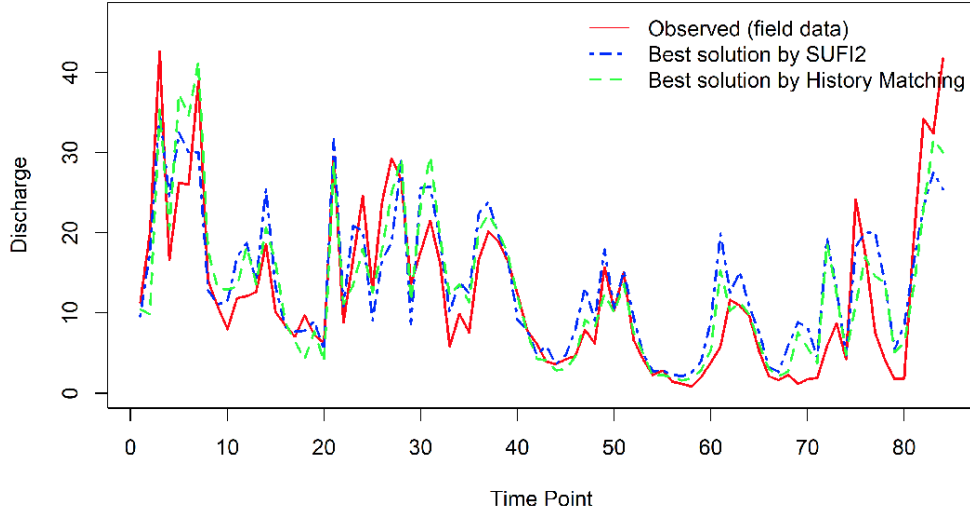


Figure 8: SWAT model calibration: The solid red curve represents the observed data, blue dashed line represents best solution using compartment model and green dashed line corresponds to the best solution using the HM algorithm.

rithm demonstrated very good performance. In Matlab-Simulink application, the HM algorithm demonstrated approximately 30% better performance than the Compartmental Model, and for SWAT model, the HM algorithm performed approximately 11% better than the proprietary software SUFI2. Thus, we believe that the proposed HM algorithm can be fruitful for solving calibration problems in time-series domain.

Note that the proposed HM approach will find the closest possible approximation in case the simulator turns out to be stochastic and cannot generate the exact same desired output  $g_0$ . Although, it is methodologically straightforward to generalize the proposed technique that can adjust for some systematic discrepancies, a bias correction step would require synchronized data on the simulator and actual field trials for multiple input combinations.

In this paper, we used the Euclidean distance approach,  $d(x) = \|g(x) - g_0\|$ , to sort through the test set for finding the inverse solution. Alternatively, one could use more sophisticated discrepancy measures, e.g., expected  $L_2$  distance, for this search.

## Acknowledgement

Ranjan’s research was supported by the Extra Mural Research Funding (EMR/2016/003332/MS) from the Science and Engineering Research Board, Department of Science and Technology, Government of India.

## References

- KC Abbaspour, CA Johnson, and MT Van Genuchten. Estimating uncertain flow and transport parameters using a sequential uncertainty fitting procedure. *Vadose Zone Journal*, 3(4):1340–1352, 2004.
- KC Abbaspour, J Yang, I Maximov, R Siber, K Bogner, J Mieleitner, J Zobrist, and R Srinivasan. Modelling hydrology and water quality in the pre-alpine/alpine thur watershed using swat. *Journal of hydrology*, 333(2):413–430, 2007.
- JG Arnold, JR Williams, R Srinivasan, KW King, and RH Griggs. Swat: Soil and water assessment tool. *US Department of Agriculture, Agricultural Research Service, Grassland, Soil and Water Research Laboratory, Temple, TX*, 1994.
- JG Arnold, DN Moriasi, PW Gassman, KC Abbaspour, MJ White, R Srinivasan, C Santhi, RD Harmel, A Van Griensven, MW Van Liew, and N Kannan. Swat: Model use, calibration, and validation. *Transactions of the ASABE*, 55(4):1491–1508, 2012.
- S Bastola and V Misra. Seasonal hydrological and nutrient loading forecasts for watersheds over the southeastern united states. *Environmental Modelling & Software*, 73:90–102, 2015.
- NV Bhattacharjee and EW Tollner. Improving management of windrow composting systems by modeling runoff water quality dynamics using recurrent neural network. *Ecological Modelling*, 339:68–76, 2016.
- Northeast Georgia Regional Commission. Northeast georgia plan 2035: Regional assessment. [http://www.negrc.org/user\\_files/1326901800\\_RegAssessmentFINAL.pdf](http://www.negrc.org/user_files/1326901800_RegAssessmentFINAL.pdf), 2011. Accessed: 2016-08-30.
- YT Dile, R Berndtsson, and SG Setegn. Hydrological response to climate change for gilgel abay river, in the lake tana basin-upper blue Nile basin of ethiopia. *PloS one*, 8(10):e79296, 2013.
- CG Dorahy, AD Pirie, I McMaster, L Muirhead, P Pengelly, KY Chan, M Jackson, and IM Barchia. Environmental risk assessment of compost prepared from salvinia, egeria densa, and alligator weed. *Journal of environmental quality*, 38(4):1483–1492, 2009.
- OJ Duncan, EW Tollner, and H Ssegane. An instantaneous unit hydrograph for estimating runoff from windrow composting pads. *Applied Engineering in Agriculture*, 29(2):209–223, 2013a.

- OJ Duncan, EW Tollner, H Ssegane, and SC McCutcheon. Curve number approaches to estimate drainage from a yard waste windrow composting pad. *Applied Engineering in Agriculture*, 29(2): 201–208, 2013b.
- RSRS Jayakrishnan, R Srinivasan, C Santhi, and JG Arnold. Advances in the application of the swat model for water resources management. *Hydrological processes*, 19(3):749–762, 2005.
- L Kalaba, BG Wilson, and K Haralampides. A storm water runoff model for open windrow composting sites. *Compost Science and Utilization*, 15(3):142–150, 2007.
- V Krysanova and R Srinivasan. Assessment of climate and land use change impacts with swat. *Regional Environmental Change*, 15(3):431, 2015.
- YH Lee and VP Singh. Tank model for sediment yield. *Water Resources Management*, 19(4): 349–362, 2005.
- J Loeppky, D Bingham, and W Welch. Computer model calibration or tuning in practice. *University of British Columbia, Vancouver, BC, CA*, 2006.
- V Picheny, D Ginsbourger, Y Richet, and G Caplin. Quantile-based optimization of noisy computer experiments with tunable precision. *Technometrics*, 55(1):2–13, 2013.
- P Ranjan. Comment: Ei criteria for noisy computer simulators. *Technometrics*, 55(1):24–28, 2013.
- P Ranjan, M Thomas, H Teismann, and S Mukhoti. Inverse problem for a time-series valued computer simulator via scalarization. *Open Journal of Statistics*, 6(03):528, 2016.
- CE Rasmussen and CKI Williams. Gaussian processes for machine learning. *The MIT Press, Cambridge, MA, USA*, 38:715–719, 2006.
- J Sacks, SB Schiller, and WJ Welch. Designs for computer experiments. *Technometrics*, 31(1): 41–47, 1989.
- TJ Santner, BJ Williams, and W Notz. *The Design and Analysis of Computer Experiments*. Springer Science & Business Media, 2003.
- MS Srinivasan, P Gérard-Marchant, TL Veith, WJ Gburek, and TS Steenhuis. Watershed scale modeling of critical source areas of runoff generation and phosphorus transport. *JAWRA Journal of the American Water Resources Association*, 41(2):361–377, 2005.

EW Tollner and KC Das. Predicting runoff from a yard waste windrow composting pad. *Transactions of the ASAE*, 47(6):1953–1961, 2004.

I Vernon, M Goldstein, and RG Bower. Galaxy formation: a bayesian uncertainty analysis. *Bayesian Analysis*, 5(4):619–669, 2010.

BG Wilson, K Haralampides, and S Levesque. Stormwater runoff from open windrow composting facilities. *Journal of Environmental Engineering and Science*, 3(6):537–540, 2004.

## Supplementary Material

### Gaussian Process Model

For this section, we assume that the simulator is deterministic, stationary and returns a scalar response  $y(x)$  for every input  $x \in [0, 1]^d$ . Sacks et al. [1989] pioneered the use of a GP model for building a surrogate for such a simulator response. Since then several variations have been proposed (see Santner et al. [2003], Rasmussen and Williams [2006] for a review). The simplest and yet the most popular version of the GP model for  $n$  training points,  $(x_i, y_i), i = 1, 2, \dots, n$ , assumes that

$$y(x_i) = \mu + Z(x_i), \quad i = 1, 2, \dots, n,$$

where  $\mu$  is the mean term and  $Z(x)$  is a GP with  $E(Z(x)) = 0$  and spatial covariance structure defined as  $Cov(Z(x_i), Z(x_j)) = \Sigma_{ij} = \sigma^2 R(\theta; x_i, x_j)$ , denoted by  $Z(x) \sim GP(0, \sigma^2 R)$ . Instead of a constant mean  $\mu$ , one can use a mean function  $\mu(x)$ . The most important component of the GP model, which makes it very flexible, is the correlation structure. Gaussian correlation is the most popular because of its properties like smoothness and usage in other areas like machine learning and geostatistics, whereas, both power-exponential and Matérn can be thought of as generalizations of the Gaussian correlation. The power-exponential correlation is given by

$$R(x_i, x_j) = \exp \left( - \sum_{k=1}^d \theta_k |x_{ik} - x_{jk}|^{p_k} \right), \quad (1)$$

where  $0 < p_k \leq 2$  are the smoothness parameters, and  $\theta = (\theta_1, \dots, \theta_d)$  measures the correlation lengths or the strength of long-range and short-range dependencies. Gaussian correlation corresponds to  $p_k = 2$  for all  $k = 1, 2, \dots, d$ . This model can be fitted either via the maximum likelihood estimation (MLE) or a Bayesian approach. Under the Bayesian framework, posterior mean prediction of  $y(\mathbf{x}^*)$  (or equivalently  $\hat{y}(x^*)$  under the likelihood method) is

$$E[y(\mathbf{x}^*)|y_1, \dots, y_n] = \mu + \mathbf{r}(\mathbf{x}^*)^T \mathbf{R}^{-1}(\mathbf{y} - \mu \mathbf{1}_n), \quad (2)$$

where  $\mathbf{r}(\mathbf{x}^*) = [\text{corr}(z(x^*), z(x_1)), \text{corr}(z(x^*), z(x_2)), \dots, \text{corr}(z(x^*), z(x_n))]^T$ ,  $\mathbf{1}_n$  is a vector of ones of length  $n$  and the associated uncertainty (posterior variance) is

$$Var[y(\mathbf{x}^*)|y_1, \dots, y_n] = \sigma^2 (1 - \mathbf{r}(\mathbf{x}^*)^T \mathbf{R}^{-1} \mathbf{r}(\mathbf{x}^*)). \quad (3)$$

In practice, the parameters  $\mu, \sigma^2$  and  $\theta$  in Equations (1), (2) and (3) are replaced by their estimates.



### Scalarization Method

From this section onwards, we again assume that the simulator under consideration generates time-series response  $g(x) = \{g(x, t), t = 1, 2, \dots, T\}$ , for any input  $x$ . Recall our objective is to find the set (or sets) of  $x$ 's that gives the perfect match or the best approximation of  $g_0$ . The main idea of the so-called scalarization method is to transform this inverse problem into a minimization problem, i.e., to find the minimizer of

$$y(x) = \|g(x) - g_0\| = \left[ \sum_{t=1}^T |g(x, t) - g_0(t)|^2 \right]^{1/2}.$$

If the target response  $g_0$  is indeed a realization of the simulator output, a perfect match can be found, otherwise, the minimization approach would lead to an approximation. Instead of using a Euclidean distance between  $g(x)$  and  $g_0$ , one could also use Mahalanobis distance, or some other discrepancy measure more suitable from a time-series standpoint. On a cautionary note, a biased or inaccurate simulator may lead to undesirable minimizer, and the computational cost of evaluating  $y(x)$  is the same as that of  $g(x)$ .

Since only a limited number (say  $N$ ) of evaluations of  $g(x)$  (and consequently,  $y(x)$ ) is allowed, this minimization problem is much trickier than the standard global optimization in mathematics, computer science and machine learning literature. Jones et al. (1998) developed an innovative merit-based criterion within a sequential design framework for efficiently estimating the global minimum of a deterministic simulator with scalar-valued response. We apply this technique on the scalarized response  $y(x) = \|g(x) - g_0\|$  and find the inverse solution. The key steps are as follows:

1. *Choose a space-filling design of size  $n < N$  (total budget of the training set),  $\{x_1, x_2, \dots, x_n\}$  from  $\chi = [0, 1]^d$ . We considered maximin Latin hypercube designs (McKay, Beckman and Conover (1979), Morris and Mitchell (1995)) in this paper.*
2. *Evaluate the simulator at the training points  $\{x_1, x_2, \dots, x_n\}$ . In our case, the simulator of interest is  $y(\cdot) = \|g(\cdot) - g_0\|$ .*
3. *Fit an appropriate statistical surrogate to  $\{(x_i, y(x_i)), i = 1, 2, \dots, n\}$ . As in Ranjan et al. (2016), we investigated the use of GP model for emulating  $y(x)$ .*
4. *If  $n < N$ , go to Step 5, otherwise go to Step 7.*
5. *Evaluate the infill-criterion on a large test set of size  $M$ . Similar to Jones et al. (1998), we used the expected improvement (EI) criterion for choosing the next trial location, i.e.,*

$$x_{new} = \underset{x \in [0, 1]^d}{\operatorname{argmax}} E[I(x)],$$

where the improvement function,  $I(x) = \max\{d_{y,min} - d_y(x), 0\}$ , is designed with the objective of finding global minimum. Under the GP model framework,  $E[I(x)]$  has a closed form expression under the predictive distribution,  $y(x) \sim N(\hat{y}(x), s^2(x))$ , that is,

$$E[I(x)] = s(x)\phi(u(x)) + (f_{min} - \hat{y}(x))\Phi(u(x)),$$

where  $u(x) = (f_{min} - \hat{y}(x))/s(x)$ , and  $f_{min}$  is the current best estimate of the global minimum.

6. *Augment the training set as  $X = X \cup \{x_{new}\}$  and  $Y = Y \cup \{y(x_{new})\}$ . Set  $n = n + 1$  and go back to Step 3.*
7. *Extract the final solution – the minimizer of  $\hat{y}(x)$ .* This is the desired inverse solution, or the best approximation we can get based on the model and data.

The step-by-step algorithm outlined here can be further generalized to accommodate a bigger class of simulators, or device a more efficient algorithm as needed by the application at hand. For instance, in Step 1, one can use another space-filling design scheme, e.g., uniform designs, orthogonal arrays, minimum coordinate correlation design, etc. (see Santner et al. [2003] for an overview). To our knowledge, there is no golden rule of selecting the right fraction for  $n/N$ , as the ideal choice may vary with the complexity of the simulator and the input dimension, it is common to take  $N/4 \leq n \leq N/2$ .

In Step 3, if any of the assumptions regarding the simulator (e.g., deterministic, stationarity, etc.) are violated, the predictive distribution and hence the functional form of the EI criterion in Step 5 may change, see for instance, Picheny et al. [2013], Ranjan [2013].

### *An Illustrative Example*

Suppose the computer simulator we wish to calibrate has two parameters, or equivalently, takes two dimensional inputs,  $x = (x_1, x_2) \in [0, 1]^2$ , and returns a time-series output,

$$g(x, t) = \frac{\sin(10\pi t)}{p_1 t} + |t - 1|^{p_2}, \tag{4}$$

where  $t = 0.5, \dots, 2.50$  (equidistant time points such that  $T = 100$ ), with  $p_1 = 1 + 2x_1$  and  $p_2 = 2 + 4x_2$ . The dashed (black) curves in Figure 9 shows a few random model outputs. Further assume that the true value of the calibration parameter is  $x_0 = (0.5, 0.5)$ , which generates the target response  $g_0$  in the inverse problem context – the solid red curve in Figure 9.

Pretending we do not know  $x_0$ , our objective here is to find  $x \in [0, 1]^2$  such that  $g(x) \approx g_0$ . We apply both the scalarization method and the modified history matching algorithm for solving

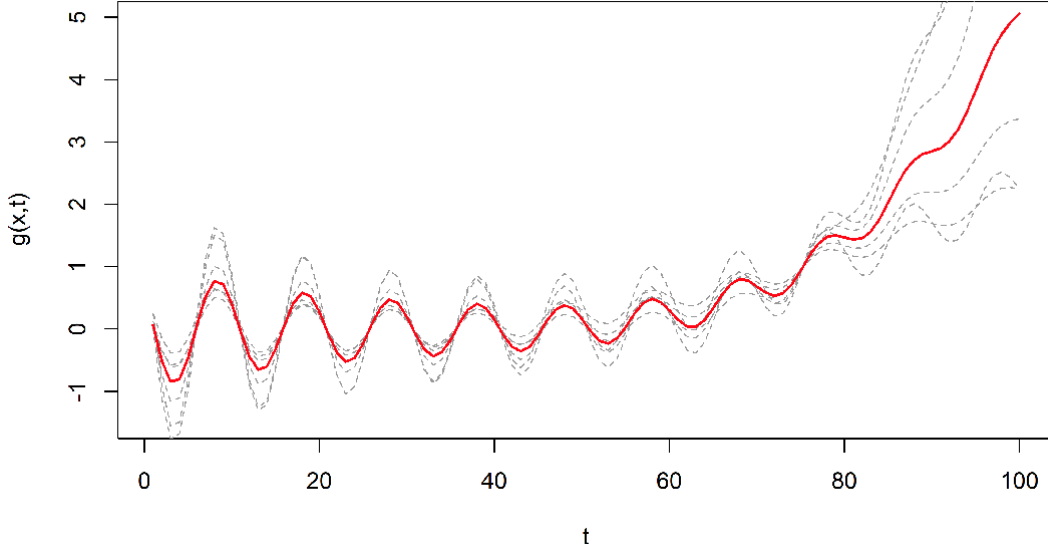


Figure 9: The illustrative example: five model outputs (dashed – in black) and the target response (solid – in red).

the inverse problem. Figure 10 presents an illustration of the scalarization method with the initial design size,  $n_0 = 10$ , total budget  $N = 40$  and the size of the test set  $M = 5000$ , where the scalarized simulator  $y(x) = \|g(x) - g_0\|$  is emulated via the GP model.

Figure 10 shows the contour plots of  $\hat{y}(x)$  fitted to  $n$  training points with  $n_0$  initial design points and  $n - n_0$  follow-up points chosen sequentially as per the EI criterion. Figure 10(a) shows the surface after adding one follow-up point, (b) and (c) show the estimated surface after 6 and 9 points have been added, respectively. Finally Figure 10(d) plots the estimated minimized  $y(x)$ . Figure 10 demonstrates that the scalarization method works reasonably well and leads to a good approximation of the global minimum of  $y(x)$ . The inverse solution (or the calibration parameter) can be estimated by  $\operatorname{argmin}\{y(x_1), \dots, y(x_n)\} = x_{opt} = (0.5059, 0.4995)$ .

It is reasonable to assume that the efficiency of the scalarization method can be optimized by judiciously choosing a few items like  $n_0$  and  $M$ . We conducted a simulation study and compared the average performance in minimizing  $y(x)$  based on 100 replications for all possible combination of  $n_0 = 5, 10, 20$  and  $M = 500, 2000, 5000$ . For each simulation the total budget for the training set is fixed  $N = 40$ , and the initial training sets and the test sets were randomly generated. Figure 11 depicts the median value of the minimized  $\log(y(x))$ . It is clear from Figure 11 that the larger the test set size, the better the average performance is, i.e.,  $M = 5000$  is the best option. Moreover, the different choice of  $n_0$  do not seem to make much difference. Of course, the inference is based on only one example and Ranjan et al. (2016) provide a more thorough comparison.

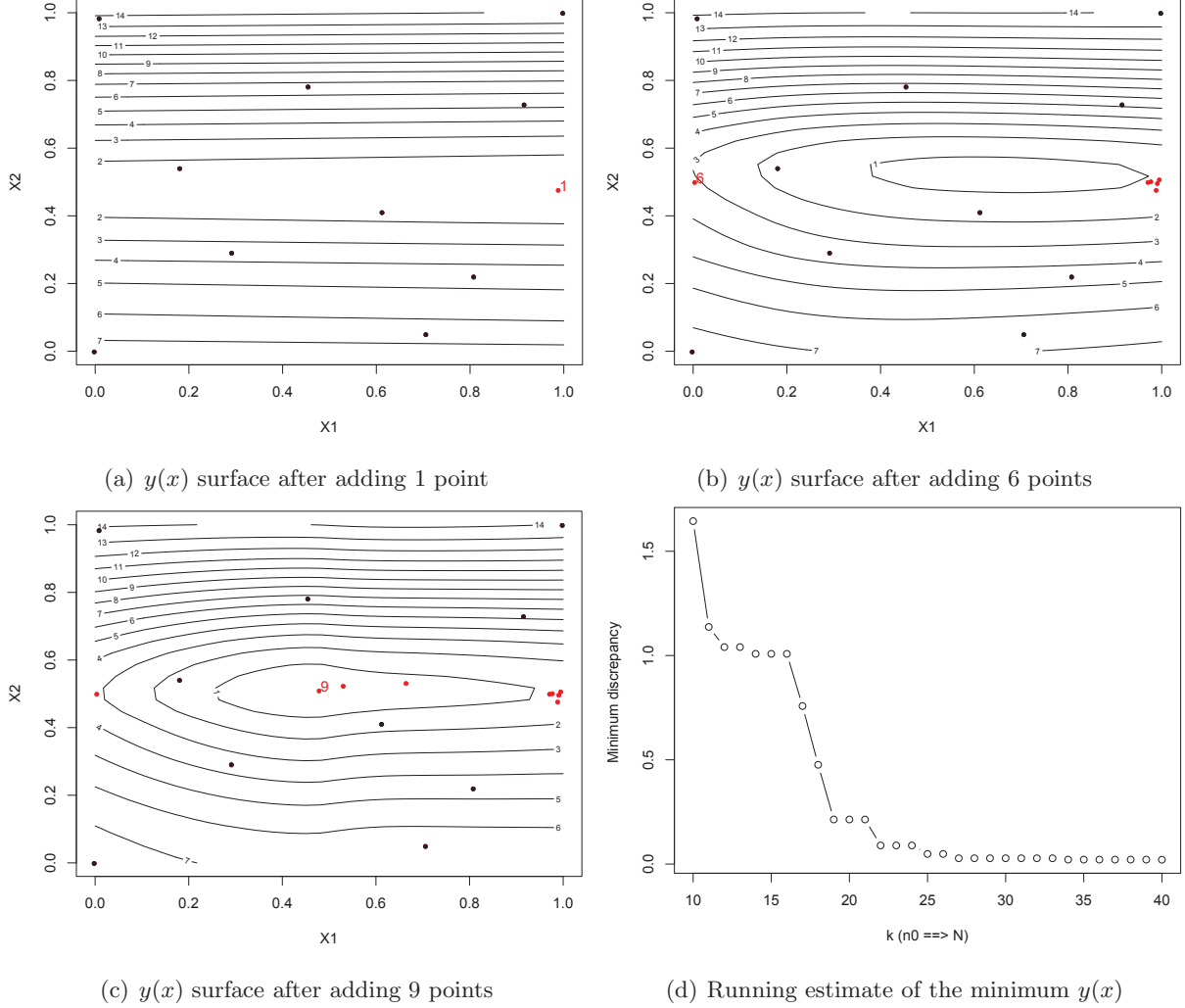


Figure 10: Calibration of the illustrative example using the scalarization method with  $n_0 = 10$ ,  $N = 40$ ,  $M = 5000$  and the GP model as the surrogate.

We now implement the history matching algorithm outlined in Section 3 for solving this inverse problem. Recall that the length of the time-series response for this simulator is  $T = 101$  and the input dimension is  $d = 2$ . Before going into the detailed discussion on the performance comparison of this methodology, we quickly illustrate the modified HM algorithm by setting the key factors to  $n_1 = 10$ ,  $c = 3$ ,  $T_k = 2$ ,  $M = 5000$  and  $DPS = (33, 67)$ . Figure 12(a) presents the selection of points in the first iteration, where the points in blue triangle and red plus correspond to  $I_{(j)}(x) \leq 3$  for  $t_1 = 33$  and  $t_2 = 67$  respectively, and the black solid circle represents  $D_2 = \{I_{max}(x) \leq 3\}$ . Figure 12(b) shows that  $D_3$  is an empty set, and hence the iterative procedure terminates.

The iterative procedure gives  $n_2 = |D_2| = 69$  (i.e., total training set size  $N = 79$ ), and the minimized  $\log[y(x_i)]$  over the training set is  $-4.2290$ . Since the median minimized  $\log[y(x_i)]$  in

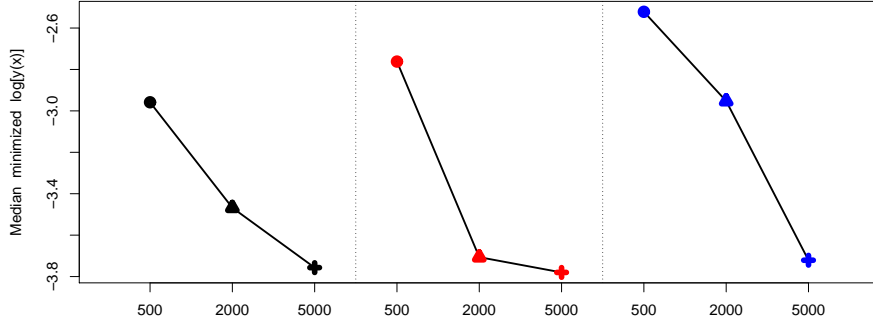


Figure 11: Performance of scalarization method - the illustrative example: The three blocks (black, red and blue) correspond to  $n_0 = 5, 10$  and  $20$ , respectively.

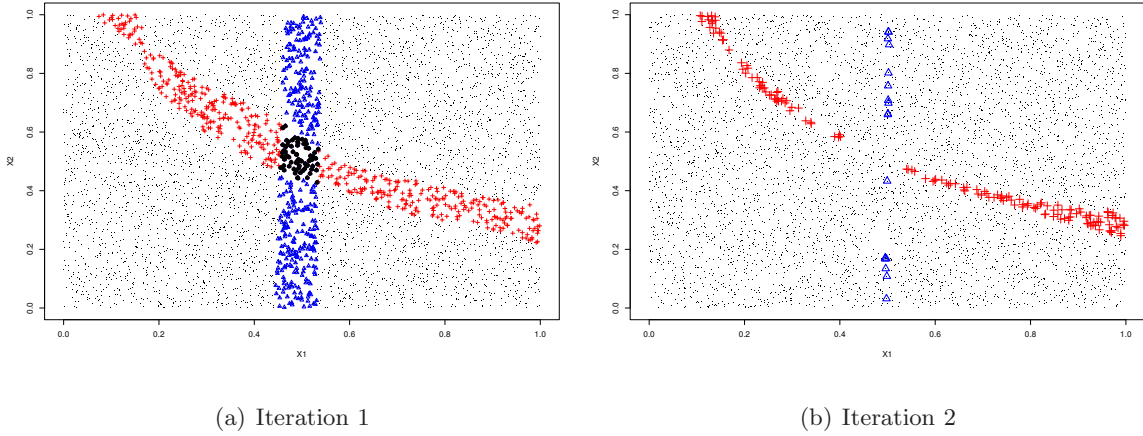


Figure 12: The illustrative example: selection of the training points according to the implausibility function at the discretization-point-set  $DPS = (33, 67)$  in the modified HM algorithm.

Figure 11 is less than  $-3.75$  (approx), it appears that HM approach gives more accurate inverse solution as compare to the scalarization method. Of course, this inference is based on one example and perhaps a more thorough investigation is required for a conclusive remarks if at all possible.

As in the scalarization approach, we conducted a simulation study for comparing the sensitivity of  $n_1, T_k, c, M$  and the DPS w.r.t. the minimization of  $\log[y(x_i)]$ . We randomly regenerate the initial training sets, test sets and the DPS for each combination of  $n_1 = (5, 10, 20), T_k = (2, 4, 8), M = (500, 2000, 5000)$  and  $c = (1, 2, 3)$ , and ran the modified HM algorithm. Figure 13 presents the marginal distribution of the median of the minimized  $\log[y(x_i)]$  for all possible two-factor combinations of  $n_1, T_k, M$  and  $c$ . For instance, the top left panel of Figure 13 shows three blocks of results for  $(M, n_1)$  in the order of  $[(500, 5), (2000, 5), (5000, 5)], [(500, 10), (2000, 10), (5000, 20)],$

and  $[(500, 20), (2000, 20), (5000, 20)]$ . These points represent the medians of the minimized  $\log[y(x_i)]$  values marginalized (i.e., averaged) over the remaining factors  $T_k$  and  $c$ .

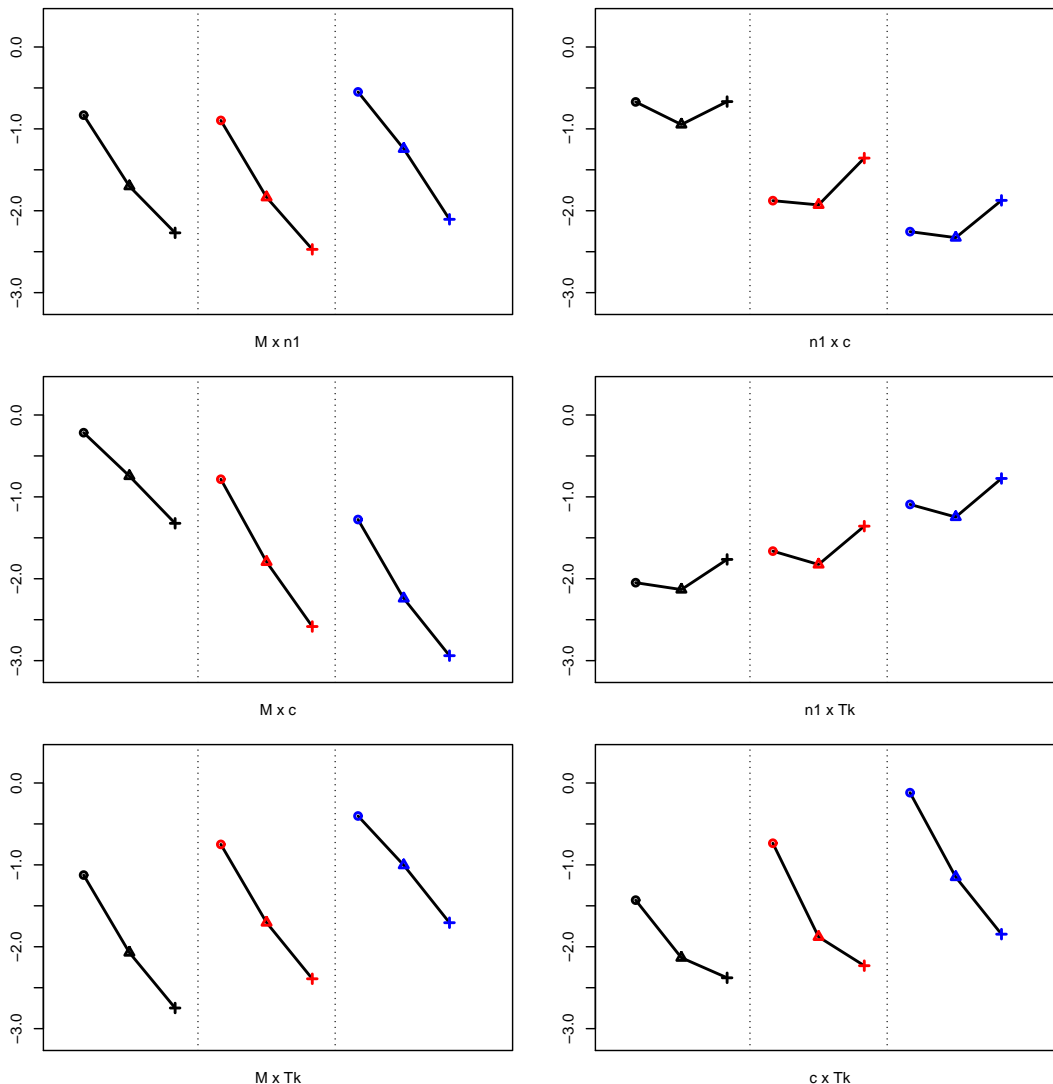


Figure 13: The illustrative example: marginal distribution of the median of the minimized  $\log[y(x_i)]$  over 100 simulations for different two-factor combinations of  $n_1, T_k, M$  and  $c$ .

From Figure 13 we can draw some inference regarding the sensitivity and preference for the key factors. For example, the top-left panel shows that  $M = 5000$  is the best choice, but there is no clear preference for  $n_1$ ; mid-left shows  $M = 5000$  and  $c = 3$  are the best options; bottom-left indicates  $M = 5000$  and  $T_k = 2 (\gtrsim 4)$  as the desirable choices; top-right shows  $n_1 = 5 \approx 10 > 20$  and  $c = 3$  as the preferred options; mid-right recommends  $n_1 = 5 \approx 10 > 20$  and  $T_k = 2$  as the best value; and the bottom-right panel depicts  $c = 3$  to be best option with  $T_k = 2 \gtrsim 4 > 8$ . In

summary, the simulation study suggests  $M = 5000$ ,  $c = 2$  as the best options with some preference for  $T_k = 2 \gtrsim 4$ , and no obvious trend for  $n_1$ .

Though we have thoroughly investigated the impact of  $T_k$ , the actual discretization-point-set (DPS) and the choice of initial design may have an impact on the total number of training points ( $N$ ) used and the precision achieved in optimizing  $\log[y(x_i)]$ . Figure 14 summarizes the impact of varying DPS and the initial training set by fixing  $T_k = 2$ ,  $c = 3$ ,  $n_1 = 10$ . The performance is measured by both the optimized  $\log[y(x_i)]$  and the total run-size.

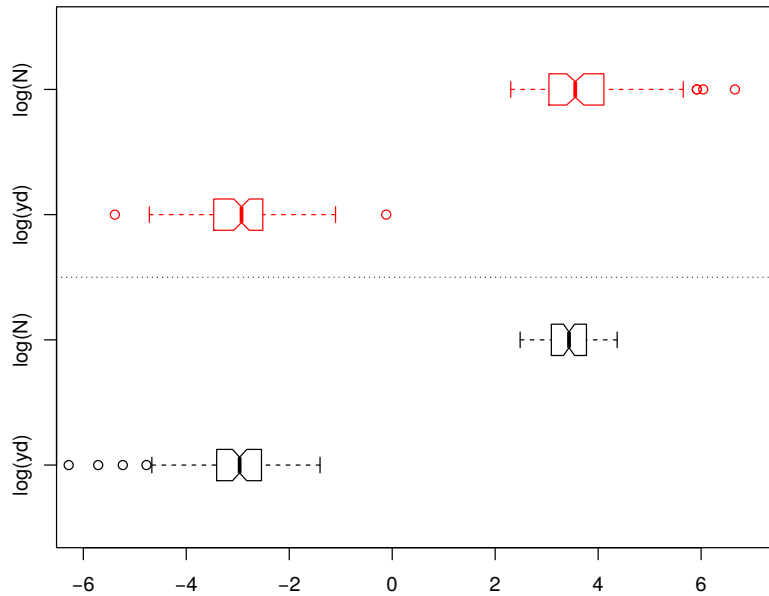


Figure 14: The illustrative example: Effect of DPS and initial design on the total run-size and optimized  $\log[y(x_i)]$ . Top block of the plot corresponds to simulations with fixed initial design (of size  $n_1 = 10$ ) and variable DPS, and the bottom panel shows the results for fixed  $DPS = (33, 67)$  and variable initial design of size  $n_1 = 10$  each.

It is clear from Figure 14 that, given a budget for the training set, the HM algorithm is not severely affected by the choice of design, but quite sensitive to the choice of DPS. The boxplot for  $\log[y(x)]$  in the top panel of Figure 14 has larger spread and right skewed. Thus, one should be careful in choosing DPS that can capture the key features of the response series.